Biochemistry

pubs.acs.org/biochemistry Article

FRET Probes for Detection of Both Active and Inactive Zika Virus Protease

Kristalle G. Cruz, Kevin Alexander, Sparsh Makhaik, and Jeanne A. Hardy*

Cite This: *Biochemistry* 2024, 63, 3300−3309 Read Online

ACCESS | Metrics & More | Article Recommendations | Supporting Information

ABSTRACT: Proteases are a privileged class of enzymes due to their catalysis of an irreversible post translational modification, namely cleavage of substrate proteins. Protease activity is essential for human pathways including inflammation, blood clotting, and apoptosis. Proteases are also essential for the propagation of many viruses due to their role in cleavage of the viral polyprotein. For these reasons, proteases are an attractive and highly exploited class of drug targets. To fully harness the power of proteases as drug targets, it is essential that their presence and function are detectable throughout the course of the protease lifetime, from inactive zymogen to the fully cleaved (mature) protease. A number of methods for detection of proteases have been developed, however, many rely on catalytic activity, so are not useful throughout the proteolytic life cycle. Here, we build on our observation that the MH1 family of benzofuran-aminothiazolopyridine inhibitors of Zika virus protease (ZVP) undergo a unique FRET interaction with tryptophan residues in the protease. The full FRET signal is only observed in higher potency binding interactions. Moreover, this approach can distinguish two inactive variants of ZVP based on their folded or unfolded state. These studies also probe the physicochemical basis of the FRET signal. Exploiting these types of FRET interactions may offer an orthogonal approach for detection of this protease, which takes advantage of the relationship between the novel ligand and the core of the protein and is therefore useful throughout the protease maturation cycle. Depending on chemical properties, this approach may be applicable in other proteases and other protein classes.

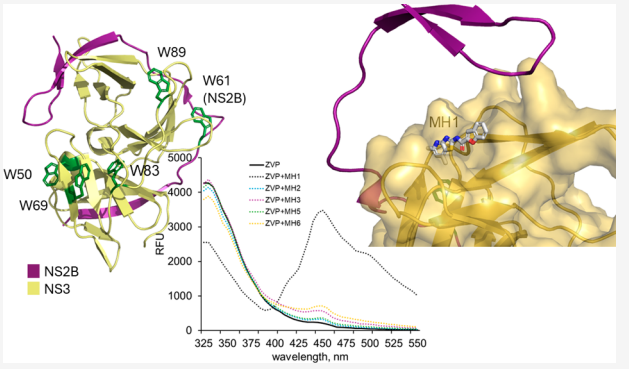

INTRODUCTION

Several methods exist for direct protease detection and for the detection of prior protease activity (cleaved substrates). Some primary tools used to detect proteases include fluorogenic substrates[1,2] and activity-based probes,[3,4] both of which rely on reaction with the protease catalytic nucleophile to perform proteolytic cleavage or covalently conjugate a fluorophore or biotin. The detection of prior protease activity is accomplished by an arsenal of tools to detect protease cleavage (for review[5]). While these methods are extremely powerful, they are not applicable in every situation, including when the protease catalytic nucleophile has been compromised or is occluded. In addition, many means of protease detection are ineffective prior to zymogen activation or when a protease is blocked by an inhibitor, such as a serpin[6,7] or an IAP.[8−11] Here, we report observation of a detectable FRET signal that is only formed upon stable ligand binding, which may be of utility in detection of target proteases regardless of their catalytic competence.

Förster resonance energy transfer (FRET) is nonradiative transfer of excitation energy from a donor fluorophore to an acceptor fluorophore. The efficiency of this energy transfer process is contingent upon several factors, including the degree of overlap between the emission spectrum of the donor and the absorption spectrum of the acceptor, the quantum yield of the donor, the relative orientation of the transition dipole moment of the donor and acceptor, as well as the spatial separation between the donor and acceptor molecules.[12,13] FRET is highly distance-dependent, with an efficiency of 50% at the Förster distance, which enables distance measurements between the donor and acceptor.[14] Even without the calculation of the donor−acceptor distance, the observation of FRET is sufficient to provide information regarding binding of a ligand.

FRET is widely acknowledged as a versatile tool for investigating interactions between proteins and ligands, as well as for elucidating protein conformational changes and dynamics.[15−19] Typically, FRET assays employ one fluorophore tethered to a protein and another to a small molecule or protein ligand or to a distal region within the same protein. However, this dual-fluorophore approach presents challenges due to potential heterogeneity and the risk of structural and functional

Received: July 19, 2024
Revised: November 7, 2024
Accepted: November 14, 2024
Published: November 26, 2024

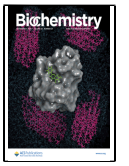

https://doi.org/10.1021/acs.biochem.4c00415
Biochemistry 2024, 63, 3300−3309

changes through fluorophore conjugation.[20] To circumvent these issues, some studies have leveraged intrinsic fluorescence stemming from aromatic amino acids, notably tryptophan residues, which are present in most proteins. In theory, the tryptophan residues in any protein could potentially act as intrinsic FRET donor(s). While optimally excited at 280 nm, tryptophan can be selectively excited over tyrosine at 295 nm with λ_{max} for emission at ∼350 nm.[21] By introducing a specific fluorescent ligand as an analytical probe for a native protein, where tryptophan residues act as intrinsic FRET donors and the ligand as the acceptor, a FRET-based fluorometric assay becomes feasible upon selective tryptophan excitation. In this work we use Zika virus protease as an exemplar to provide insights into how small molecule inhibitors may also serve as robust FRET reporters for the presence of the unmodified, native protease.

Zika virus, which belongs to the flavivirus family, has a positive-sense RNA genome that is translated into a polyprotein. The polyprotein is then cleaved by both host[22−24] and viral proteases[25−29] to release the structural and nonstructural proteins, a process that is important for maturation of the virus. Consequently, targeting the viral protease emerges as a promising strategy for the development of therapeutic inhibitors against Zika virus and related pathogens.

Zika virus protease (ZVP) consists of the chymotrypsin-like protease domain (NS3pro) and a short NS2B "cofactor" region, which is necessary for NS3pro's stability and proteolytic activity.[30] After the self-cleavage of the NS2B-NS3 complex, NS2B recruits NS3 to the ER membrane, where NS3's protease activity is activated through its interaction with the C-terminal region of NS2B.[31] We previously reported MH1, an allosteric inhibitor that exhibits an IC_{50} of 440 nM and specificity for ZVP compared with other flaviviral proteases.[32] In addition, MH1 was greater than 5-fold more effective at preventing viral infection of zika virus than the other flaviviruses tested including dengue serotype 2, Japanese encephalitis, Powassan, Usutu, West Nile, and yellow fever viruses, as assessed by the cytopathic effect (CPE) assay. In the present study, we observed significant FRET between ZVP's intrinsic tryptophan residues and MH1. This FRET was not observed with other flaviviral proteases such as Dengue virus protease (DVP) and West Nile virus protease (WNVP). Moreover, a correlation emerges between the observed FRET and the extent of inhibition observed for other MH analogs. This correlation extends to MH1's inhibition against ZVP variants, suggesting the potent utility of MH1 for making FRET measurements to probe binding interactions.

RESULTS AND DISCUSSION

MH1 has emerged as an interesting probe for Zika virus protease due to its potency and selectivity.[32] We have carried out investigations of the properties of MH1 to uncover more details of its mechanism of inhibition and its potential as a therapeutic. One of the most surprising observations of MH1 behavior is its ability to serve as a FRET acceptor when bound to ZVP. MH1 itself is very weakly excited by 295 nm light. Tryptophan is known to be readily excited at 295 nm. ZVP excited at 295 nm produces a strong 340 nm fluorescence emission (Figure 1A). Selective excitation (295 nm) of the tryptophan residues of MH1-bound ZVP resulted in a strong MH1 emission peak centered at 460 nm together with quenching of the tryptophan direct emission peak at 340 nm (Figure 1A). MH1 is not significantly excited by 295 nm excitation (Figure 1B), but is excited by wavelengths from 330 to 370 nm. The red-shifted

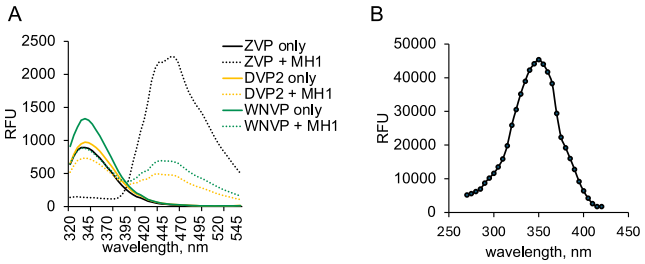

Figure 1. FRET is observed between the tryptophan residues of ZVP and compound MH1. (A) Emission spectra of ZVP, DVP2, and WNVP incubated with MH1. An excitation wavelength of 295 nm was used to selectively excite the tryptophan residues. (B) Excitation spectrum of MH1. Emission was recorded at 460 nm.

location of the ZVP-MH1 emission peak relative to the tryptophan emission peak confirms the status of MH1 as the FRET acceptor. The increased fluorescence signal of ZVP-bound MH1 is consistent with binding of a fluorophore to a hydrophobic cavity, which has been shown in a number of cases to significantly increase fluorescence.[33−36] These data suggest that MH1 comes into close contact with one or more tryptophan residues, facilitating robust energy transfer. This spectral pattern can only be observed for ZVP and not with other flavivirus proteases such as DVP2 and WNVP (Figures 1 and S1A−C), although the tryptophan residues are conserved in all three flaviviral proteases (Figure S1D). This observation might be expected since MH1 demonstrates a markedly weaker binding affinity toward DVP2 (IC_{50} = 22 μM) and WNVP (IC_{50} = 6.9 μM) compared to ZVP (IC_{50} = 0.44 μM).[32]

To assess the impact of each tryptophan on the observed FRET, each ZVP tryptophan residue was replaced by phenylalanine and the new ZVP variants were incubated with MH1. Phenylalanine is structurally similar to tryptophan, but has 5-fold lower fluorescence quantum yield than tryptophan, making Trp to Phe substitutions an effective means of assessing the contributions of tryptophan to the observed FRET interaction.[20] The Trp to Phe substitution experiment also aimed to identify the potential binding site of MH1 by assessing changes in the ZVP emission spectrum. ZVP has five tryptophan residues. One can be found in the NS2B cofactor and the rest in the NS3 core (Figure 2A). Expression of most Trp to Phe variants led to no changes or modest differences in protein expression level and activity (Figure 2B,C). However, the W89F substitution resulted in exceedingly low protein expression (data not shown). Incubating tryptophan-substituted variants of ZVP with MH1 did not lead to any significant changes in the appearance and intensity of the MH1 emission peak (Figures 2D,E and S2) indicating that all tryptophan residues are contributing to the observed FRET, as is consistent with a molecular orbital view of the electronic structure of ZVP. Because W61 resides at the NS2B-NS3 interface, we were particularly interested in whether substitution of this residue would impact the observed FRET. Importantly, W61F retains FRET between the protein and MH1 suggesting that it is not simply alteration of the W61 chemical environment or conformation that results in the observed signal, but is indeed FRET. To promote at least 50% efficient energy transfer via FRET, the distance between the donor and the acceptor is typically in the range of 2−6 nm.[12] In extant structures of ZVP,[37−43] the longest axis across the protein measures around ∼4.5 nm. Our prior work suggests that MH1 binds competitively with NS2B residues 67−83.[32] The four tryptophan substituted

https://doi.org/10.1021/acs.biochem.4c00415
Biochemistry 2024, 63, 3300−3309

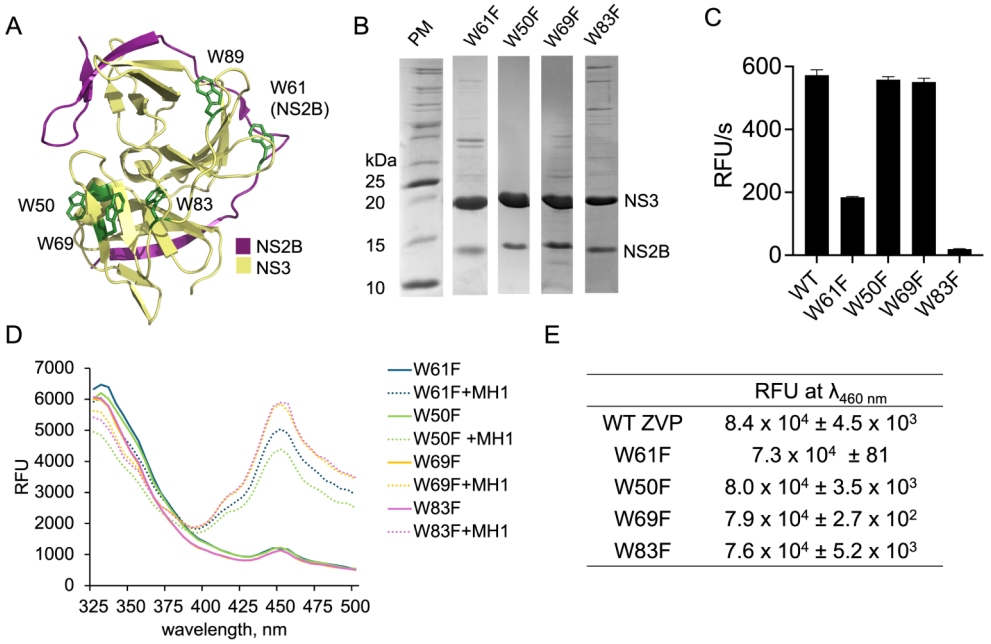

	RFU at $\lambda_{460\ nm}$
WT ZVP	$8.4 \times 10^4 \pm 4.5 \times 10^3$
W61F	$7.3 \times 10^4 \pm 81$
W50F	$8.0 \times 10^4 \pm 3.5 \times 10^3$
W69F	$7.9 \times 10^4 \pm 2.7 \times 10^2$
W83F	$7.6 \times 10^4 \pm 5.2 \times 10^3$

Figure 2. Trp to Phe substitutions in ZVP suggest that all the tryptophan residues contribute to the FRET observed between ZVP and MH1. (A) ZVP structure (PDB: 5H4I) depicting the NS2B cofactor (purple) and NS3pro core domain (yellow) with tryptophan residues colored in green. (B) SDS-PAGE gel of the purified Trp to Phe variants. (C) Phenylalanine substitutions result in differences in the activity of ZVP. (D) Emission spectra of ZVP W → F mutants incubated with MH1. (E) RFU values measured at $\lambda_{460\ nm}$ for each ZVP W → F mutants incubated with MH1.

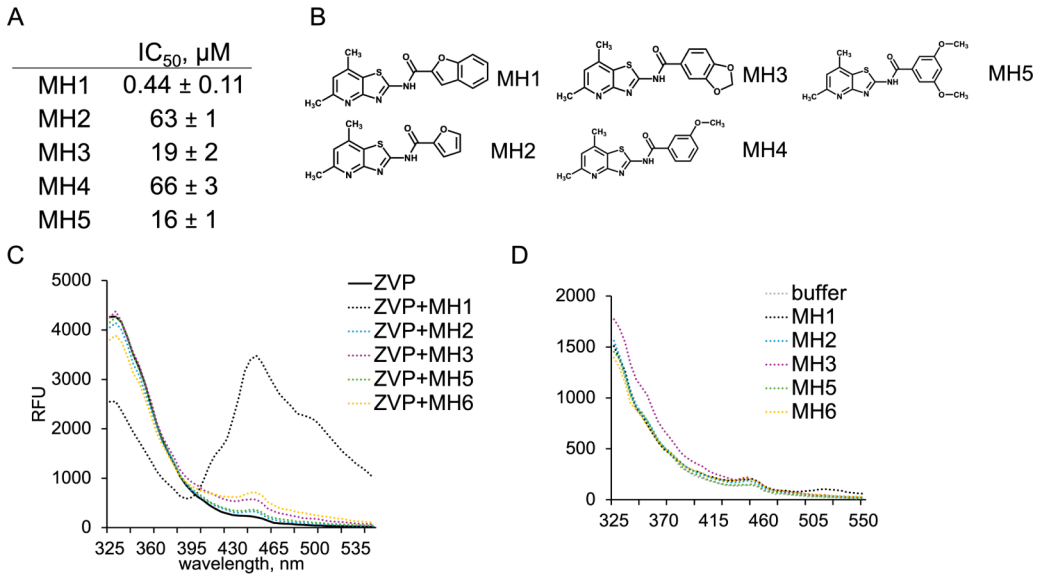

	IC_{50}, μM
MH1	0.44 ± 0.11
MH2	63 ± 1
MH3	19 ± 2
MH4	66 ± 3
MH5	16 ± 1

Figure 3. At low inhibitor concentration, FRET can only be observed between ZVP and MH1 but not weaker inhibitors. (A) IC_{50} values of different MH inhibitors for ZVP as previously reported.[32] (B) Structures of MH compounds. (C) Fluorescence emission spectra of ZVP incubated with different MH inhibitors. (D) Fluorescence emission spectra of MH inhibitors alone.

variants that could be purified are all similarly distal from this site (Figure S2E,F). Thus, without gross conformational changes occurring, these four tryptophan residues should collectively contribute to the molecular orbital of ZVP and the observed energy transfer regardless of the location of MH1 binding. These data (Figures 2D,E and S2) support the notion that no major conformational changes are required in ZVP to accommodate MH1 binding.

Emission spectra of ZVP incubated with MH-analogs (Figure 3A,B) lack the quenched 340 nm peak and the strong emission peak at 460 nm (Figures 3C and S3). Notably these analogs do not show any significant fluorescence under these conditions in the absence of ZVP (Figure 3D). For FRET from tryptophans to bound ligands to be observable, inhibitors should bind sufficiently tightly.[44] Since the MH1 analogs have IC_{50} values that are significantly weaker than MH1 (Figure 3A), it is not entirely surprising that FRET is not readily observed. However, when the concentration of compounds MH3, MH4, and MH5 are increased (Figure 4D,F and H) the resulting emission spectrum exhibits an increase in the 460 nm peak as was observed for MH1 (Figure 4C,E and G). For MH2, an increase in concentration did not translate in an increase in the 460 nm peak (Figure 4A,B). It is possible that MH2 does not fluoresce, but rather releases energy in a nonradiative process. For MH-

https://doi.org/10.1021/acs.biochem.4c00415
Biochemistry 2024, 63, 3300−3309

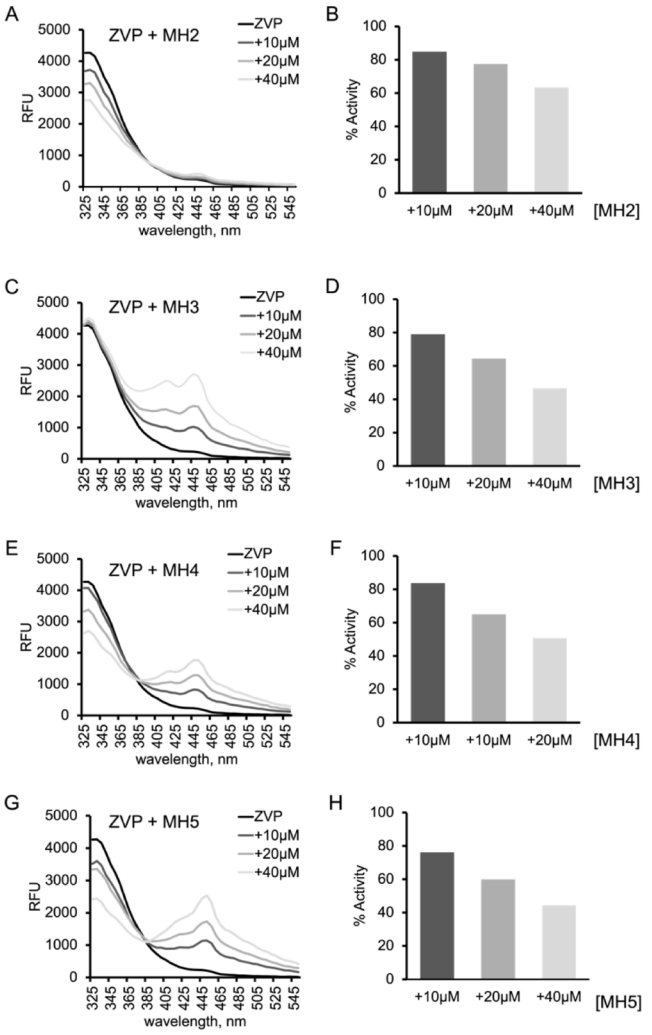

Figure 4. FRET can be observed between ZVP and MH compounds at higher inhibitor concentrations. (A, C, E, and G) Emission spectra of ZVP incubated with increasing concentrations of MH inhibitors. (B, D, F, and H) Activity of ZVP incubated with increasing concentrations of MH inhibitors.

analogs, the FRET emission intensity is roughly proportional to the magnitude of inhibition. This observation can also be seen with the emission spectrum of ZVP incubated with SM compounds (Figures 5 and S4). SM1, SM2, SM3 and SM6, which have IC_{50} values close to MH1, show an obvious increase in the 440−460 nm peak.

To elucidate the inhibition mechanism of MH1 function, we had previously constructed hybrid constructs of ZVP and DVP2.[32] ZVP^{48-100} comprises the NS3 core of ZVP bound with the NS2B region of DVP2 spanning residues 48−100. Conversely, $DVP2^{48-100}$, features the NS3 core of DVP2 bound to the NS2B region of ZVP (residues 48−100).[32] MH1 inhibition of both ZVP^{48-100} and $DVP2^{48-100}$ was ∼19-fold less potent than for WT ZVP (Figure 6A). Consistently, this reduced inhibition was reflected in minimal FRET, as demonstrated in their emission spectra (Figures 6B and S5). The utilization of weakly binding inhibitors and hybrid constructs, where MH1 binds weakly, establishes a clear correlation between binding strength and the observation of FRET (Figure S6).

Some mutations in ZVP lead to a significant reduction or complete loss of protease activity. For these cases, measuring inhibition by monitoring the activity of the protease using a fluorogenic peptide substrate is impossible. Moreover, it is impossible to distinguish whether loss of activity is due to a simple loss of catalytic activity or full unfolding of the protease. Given that binding of MH1 results in FRET, it becomes feasible to demonstrate MH1 binding to these ZVP variants by monitoring the increase in peak intensity around 460 nm. We focus on two inactivating mutations that cause inactivation by different mechanisms.

The CD spectrum of the first inactive variant F84A is highly similar to that of WT ZVP, which shows a characteristic CD spectrum for a β-sheet containing protein. This suggests that F84A remains folded (Figure 7B). In spite of showing a native like fold, F84A is catalytically inactive (Figure 7E). The F84 residue on ZVP has been shown to interact with N152 of the NS3pro and serves as an anchor for the C-terminal residues of NS2B to NS3pro (Figure 7A).[45,46] This C-terminal region is vital for substrate processing, as it forms the negatively charged S2 subsite responsible for recognizing the basic residue at the P2 position within the substrate.[47] In ZVP, the F84A mutation destabilizes the C-terminal region, rendering the enzyme incapable of processing substrates and consequently impeding our ability to monitor its activity. Incubation of ZVP F84A with MH1 results in an emission spectrum with a prominent peak at around 460 nm (Figure 7C). Binding of MH1 to ZVP F84A is observed through thermal shift assay (Figure 7D). An increase in melting temperature observed for ZVP F84A in the presence of MH1 indicates that MH1 binds to this inactive variant. Notably, these data provide a robust and measurable FRET signal despite the lack of measurable protease activity due to this substitution.

Like F84A, replacing the W61 residue in the NS2B region of ZVP leads to the inactivation of the protease (Figure 7H), but also leads to unfolding (Figure 7B). W61 plays a crucial role in stabilizing the folded form of ZVP as it anchors the N-terminal residues of NS2B to NS3pro, forming an interaction with the Q96 residue of NS3pro.[48] In WNVP, mutating either W61 or Q96 abolishes protease activity,[49,50] further indicating the importance of this region. Structural analyses of related proteases reveal that the N-terminal residues form a β-strand within the N-terminal lobe of the NS3pro region, visible in both the open and closed conformations of ZVP and similar proteases.[32] This suggests that while the C-terminal region of NS2B is dynamic, the N-terminal region of NS2B helps to retain the NS2B cofactor in complex with the NS3pro. Thus, any mutation disrupting the interaction between the N-terminal residues of NS2B with NS3pro could potentially lead to dissociation of the NS2B-NS3pro complex and hence lead to inactivity. When the ZVP W61A variant is incubated with MH1, both the emission spectrum (Figure 7F) and thermal shift (Figure 7G) behavior mirror that of the ZVP W61A alone, indicating that no binding is possible for this ZVP variant. The absence of a prominent peak at 460 nm when MH1 is added supports our prior conclusion[32] that binding of MH1 necessitates the interaction of properly folded NS2B and NS3. Most importantly, this establishes that MH1 can serve as a probe for both active and inactive ZVP so long as it is folded. This tool provides a complement to detection by traditional (non-conformationally specific) antibodies, which cannot typically distinguish folded and unfolded forms a protein.

Our FRET experiments and the previously determined IC_{50} values establish a clear partition of the MH and SM series into

https://doi.org/10.1021/acs.biochem.4c00415
Biochemistry 2024, 63, 3300−3309

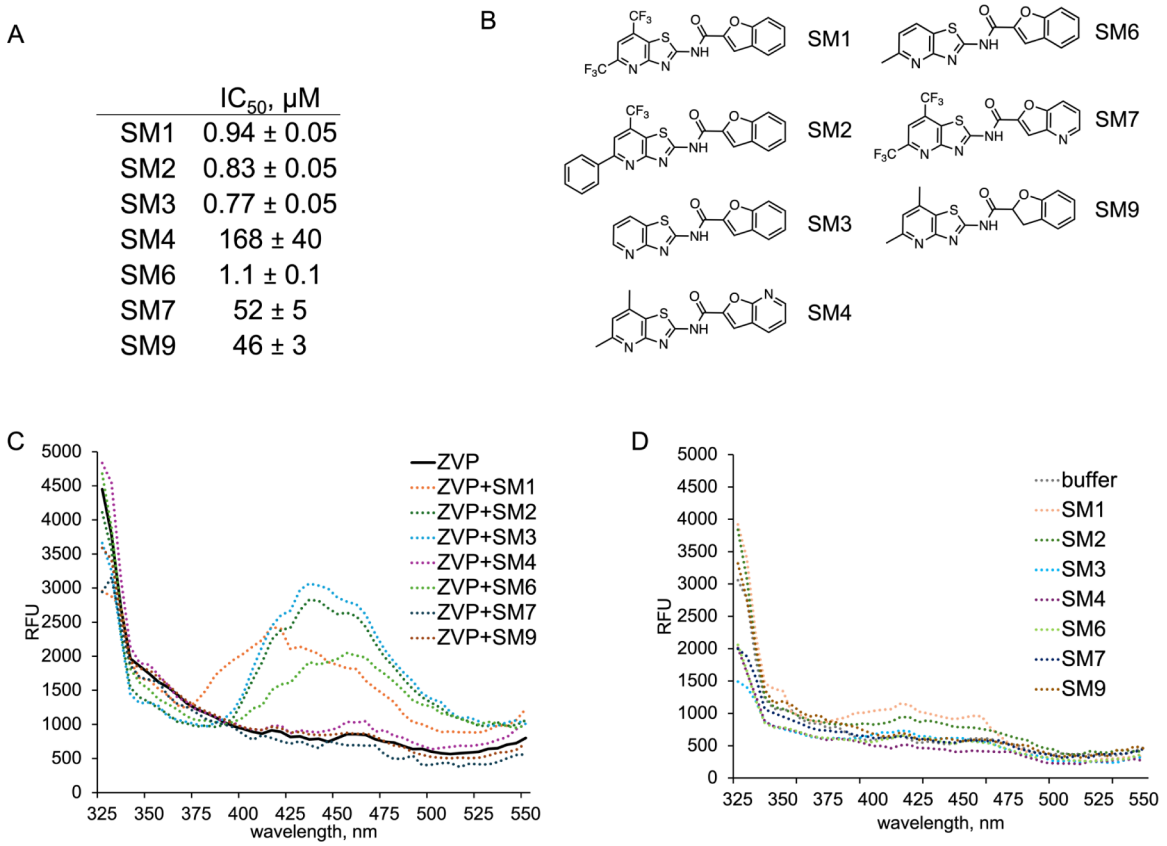

Figure 5. More potent SM compounds participate in FRET with ZVP. (A) IC_{50} values of SM inhibitors against ZVP as previously reported.[32] (B) Structure of SM compounds. (C) Emission spectra of ZVP incubated with SM inhibitors. (D) Emission spectra of different SM inhibitors.

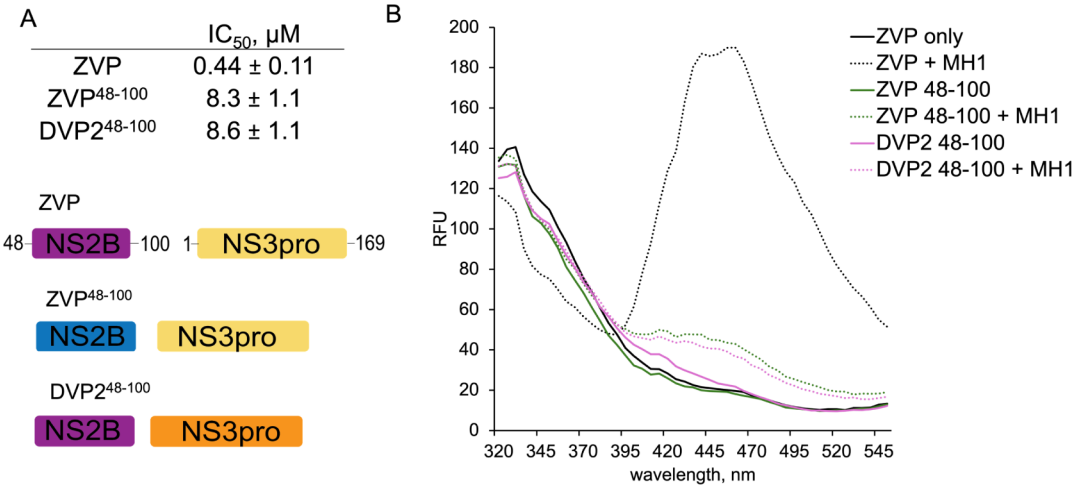

Figure 6. At low MH1 concentrations, no FRET can be observed between MH1 and the full hybrid constructs. (A) IC_{50} values of MH1 with ZVP^{48-100} and $DVP2^{48-100}$ constructs as previously reported.[32] ZVP^{48-100} has the NS3pro of ZVP and NS2B of DVP2. $DVP2^{48-100}$ has the NS3pro of DVP2 and the NS2B of ZVP. (B) Emission spectra of WT ZVP and hybrid constructs incubated with MH1.

"weak" and "strong" inhibitors. We aimed to explain the differences in inhibition potencies using density functional theory (DFT) by correlating molecular properties with IC_{50}. Among the molecular parameters assessed—HOMO−LUMO gaps, bond angles, bond lengths, and atomic partial charges—the atomic partial charge exhibited the strongest correlation with IC_{50}, (Figure 8) with planarity appearing to also be requisite for inhibition (Figure S7). Specifically, the sum of nonhydrogen partial charges of the benzene ring of the benzofuran moiety distinguishes the strong from the weak inhibitors. For strong inhibitors, the partial charge sum is around −1.0, whereas the partial charge sum is significantly more positive for weaker inhibitors (Figure S8). Although these charge predictions are likely only valid on a qualitative level, the trend in IC_{50} values [strong inhibitors] < SM9 < SM7 < SM4 reflects the trend observed for the negative partial charge sums. Note that this trend is not linear and instead IC_{50} appears to increase roughly exponentially with decreasing charge magnitude. We can

https://doi.org/10.1021/acs.biochem.4c00415
Biochemistry 2024, 63, 3300−3309

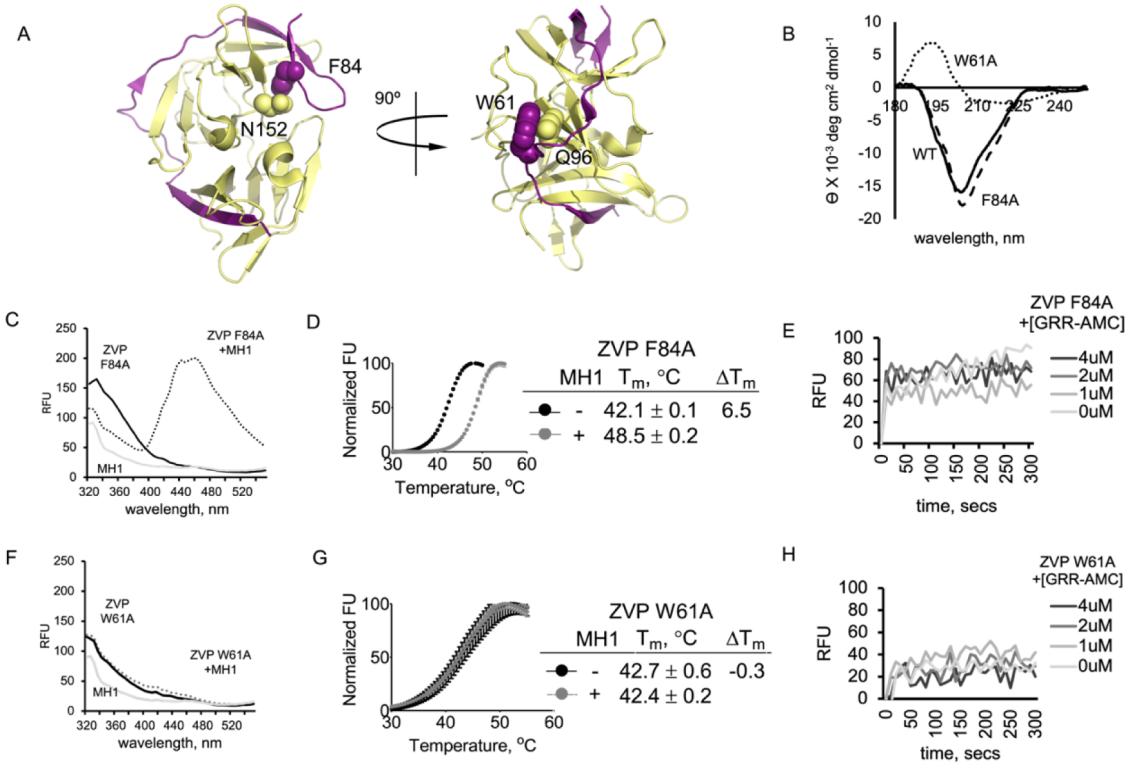

Figure 7. Binding of MH1 to inactive ZVP variants can be observed by monitoring FRET. (A) Interaction of F84 (NS2B) with N152 (NS3) is reported to stabilize the NS2B C-terminal region.[45] W61 (NS2B), is reported to interact with Q96 and serves as an anchor for the NS2B cofactor to the NS3 core.[46] (B) The CD spectra of WT ZVP, and the F84A and W61A ZVP variants. (C and F) Emission spectra of ZVP F84A or W61A incubated with MH1. (D and G) Thermal shift of ZVP F84A and W61A with and without MH1. (E and H) Activity of ZVP F84A and W61A with increasing concentrations of MH1.

rationalize this with the following assumptions: (1) IC_{50} follows K_d, (2) K_d is proportional to $e^{\Delta G}$, where ΔG corresponds with the formation of the protein−ligand complex, (3) $\Delta G \approx \Delta U_{elec}$ associated with the Coulombic attraction between the inhibitor compound and the protein binding site, assuming small changes in entropy and volume, (4) ΔU_{elec} is linearly proportional to the benzofuran benzene partial charge Q. We do not claim quantitative accuracy for this trend given the significant approximations used to model solvent effects, but this relationship at least qualitatively matches our expectations and indicates that a strongly negative benzofuran charge is necessary for potent ZVP inhibition. Together our data from the MH and SM compounds, as well as ZVP hybrids and variants underscores the promising potential of employing FRET for monitoring MH1 binding to folded proteases that are both active and inactive. In fact, FRET has been employed before in monitoring ligand binding and protein−protein interactions.[51−54] Lee and Peterson utilized FRET as a tool to quantify the binding of small molecules to proteins, employing streptavidin and biotin as their model system.[55] Streptavidin, a tetrameric protein known for its high affinity to biotin ($K_d = 10^{-14}$ M), possesses six tryptophan residues in proximity to the biotin binding site, making it ideal for FRET-based investigations into small molecule-protein interactions. They synthesized Pacific blue, acting as a FRET acceptor, and conjugated it to various analogs of biotin that displayed varying binding affinities for streptavidin. The K_d values obtained from the binding curve generated by measuring the amount of FRET observed at 460 nm correlated well with the K_d values determined via isothermal titration calorimetry.

This correlation is in line with some prior observations. In an unrelated study, Huang et al. demonstrated the measurement of binding affinity using FRET, employing the signal transducer β-arrestin-1 as their model system.[56] They incorporated a synthetic fluorescent amino acid L-(7-hydroxycoumarin-4-yl)ethylglycine (Cou) into β-arrestin-1, serving as an acceptor for the tryptophan present in Fab30. Upon interaction of active β-arrestin L293Cou with Fab30, the fluorescence of Fab30 exhibited a noticeable reduction within the 300 to 400 nm range, while displaying a significant increase in intensity at 450 nm. The binding affinity of Fab30 was determined either by saturating β-arrestin L293Cou with Fab30 or by a competition experiment where wild-type β-arrestin was introduced to the β-arrestin L293Cou/Fab30 complex. In both cases, the intensity of Cou emission was recorded, and curve fitting was employed to calculate the K_d values. Our results build on these prior observations. MH1 FRET with ZVP is a robust and accurate indicator of binding to both active and inactive variants of ZVP so long as they remain in a folded state.

CONCLUSION

These studies began with the unexpected observation that the MH1 family of inhibitors was capable of a robust FRET interaction with ZVP regardless of the activation state of the enzyme. Many proteases are initially expressed as inactive zymogens, or can be inactivated by native cellular inhibitors (e.g., IAPs and serpins). We recognized that a FRET signal could provide a useful new means of tracking the presence of proteases throughout their life cycle because, unlike most chemical tools for protease detection, they do not require an active, accessible

https://doi.org/10.1021/acs.biochem.4c00415
Biochemistry 2024, 63, 3300−3309

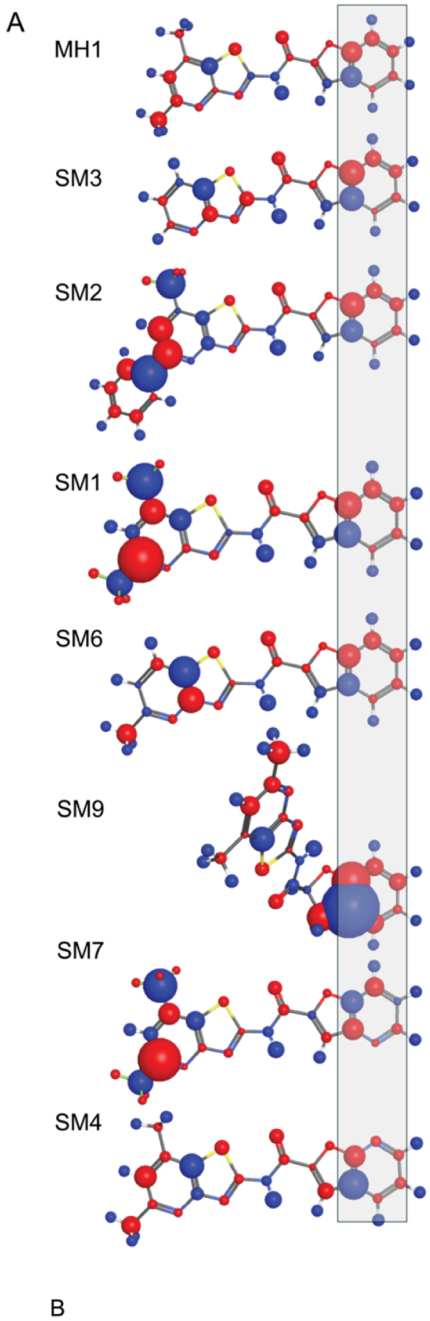

B

	IC_{50}, μM	Charge
MH1	0.44 ± 0.11	-0.98
SM3	0.77 ± 0.05	-1.02
SM2	0.83 ± 0.05	-1.06
SM1	0.94 ± 0.05	-0.98
SM6	1.1 ± 0.1	-1.08
SM9	46 ± 3	-0.84
SM7	52 ± 5	-0.65
SM4	168 ± 40	-0.39

Figure 8. Strong ZVP inhibitors have highly negative benzofuran charges. (A) Lowest energy molecular configurations and associated atomic partial charges (red = negative, blue = positive; radius corresponds with charge magnitude) as computed by DFT. The sum of nonhydrogen atoms in the benzofuran benzene ring (highlighted with the gray box) is reported in (B).

and unmodified active site. This study undertook a systematic analysis of the binding and inhibition properties of the MH1 family and correlated these observations with activity. Together these insights demonstrated that MH1 FRET with ZVP is a robust and accurate indicator of binding to both active and inactive variants of ZVP (so long as the ZVP variant remains folded). We foresee that this approach may be generalizable to other compounds with fluorescent properties similar to MH1. A fruitful direction for future studies might include development of probes such as MH1 by design rather than happenstance. A key step in that process is establishing a strong working knowledge of both the binding determinants and the characteristics that support FRET interactions with key tryptophan residues in the protein of interest. One of the most surprising findings of our work is that the FRET signal was not dependent on just one or a few of the five tryptophans in ZVP, suggesting a large working range for the MH1-ZVP FRET signal. Our computational analysis of the MH1 family of compounds also yielded useful insights. For example, we observed that for MH1, the charge on the benzofuran benzene ring is key to predicting both affinity and inhibitory properties. A high-resolution structure of the MH1-ZVP complex would undoubtedly add additional insights into this FRET system. In spite of the advantages afforded by additional structural characterization, it is clear the investigations described herein will help to lay the groundwork for the systematic design of FRET reporters for the flavivirus proteases as well as for many other protein classes.

MATERIALS AND METHODS

Plasmid Construction. Unlinked ZVP (Uniprot: Q32ZE1) was a gift from Dahai Luo (Addgene plasmid # 86846; http://n2t.net/ addgene:86846; RRID:Addgene_86846).[38] The DVP2 (Uniprot: P12823) unlinked construct was a gift from Thomas Keller.[57] In this coexpression system, gene encoding residues 48−100 of the NS2B cofactor were inserted into the Nde1/XhoI sites in a separate pACYDuet vector, while the gene encoding residues 1−187 of the NS3 protease were inserted into the NdeI/Xho sites in the pETDUET vector. Lastly, unlinked WNVP (Uniprot: P06935) construct, which is designed to allow coexpression of NS2B and NS3pro in pET28a vector, was provided by Min Chen from the Chemistry Department of University of Massachusetts Amherst. The ZVP^{48-100} hybrid was prepared simply by deleting the NS2B region in the pET15b vector for coexpression with the DVP2 NS2B region. DVP^{48-100} hybrid was constructed by amplifying the ZVP NS2B 48−100 region in the pET15b vector using restriction site overhangs for NdeI for the forward primer and XhoI for the reverse primer and inserting it into the NdeI/XhoI double restriction digested pACYDuet vector. Point substitutions in ZVP (F84A*, W61A*, W61F*, W50F, W69F and W83F) were created using site-directed mutagenesis and validated by DNA sequencing. (*Amino acids labeled with * are NS2B residues.*)

Expression and Purification. Unlinked ZVP was transformed into BL21(DE3) electrocompetent *E. coli* and plated onto LB plates with 100 μg/mL ampicillin. Unlinked DVP2 WT was cotransformed by transforming NS2B 48−100 in the pACYDuet vector with NS3pro 1−187 in the pETDUET vector and plating on LB plates supplemented with 34 μg/mL chloramphenicol and 100 μg/mL ampicillin. Unlinked WNVP was transformed into BL21(DE3) electrocompetent *E. coli* cells and plated onto LB plates with 50 μg/mL kanamycin. ZVP^{48-100} and DVP^{48-100} hybrids were cotransformed similarly to the DVP2 unlinked WT construct, however ZVP^{48-100} requires ZVP delNS2B in pET15b. ZVP F84A*, W61A*, W61F*, W50F, W69F and W83F were each transformed similarly to the unlinked ZVP. Cultures were grown in LB media with

https://doi.org/10.1021/acs.biochem.4c00415
Biochemistry 2024, 63, 3300−3309

appropriate antibiotics at 37 °C until OD_{600} reached 0.6−0.8. At this point, IPTG was added to a final concentration of 1 mM and the temperature was reduced to 25 °C for 4 h to allow protein expression. The cells were pelleted by centrifugation, stored at −80 °C, and then freeze−thawed in lysis buffer (50 mM Tris, pH 8.5, 50 mM NaCl, 5% glycerol and 2 mM imidazole) before being lysed in a microfluidizer. The lysate was clarified by centrifugation at 27,000 rcf at 4 °C for 1 h. The supernatant was loaded onto a 5 mL HisTrap nickel-affinity column (GE Healthcare) pre-equilibrated with lysis buffer. The column was washed with wash buffer (50 mM Tris, pH 8.5, 50 mM NaCl, 5% glycerol and 10 mM imidazole) before being eluted with elution buffer (50 mM Tris, pH 8.5, 50 mM NaCl, 5% glycerol, 300 mM imidazole). The eluted protein was diluted ∼5× in Buffer A (50 mM Tris, pH 8.5, 5% glycerol) and loaded onto a 5 mL HiTrap Q column (GE Healthcare). A linear NaCl gradient was used to elute the proteins using Buffer B (50 mM Tris, pH 8.5, 1 M NaCl, 5% glycerol). Protein eluted at ∼250 mM NaCl, was assessed for purity by SDS-PAGE and immediately stored at −80 °C until further use.

IC_{50} Determination. To determine the IC_{50} value for MH1 against ZVP, MH1 was serially diluted in ZVP activity assay buffer (10 mM Tris, pH 8.5, 20% glycerol, 1 mM CHAPS). ZVP at 50 nM was incubated with MH1 from 100 μM to 0.098 μM (serial dilution of 11 concentrations) for 1 h at room temperature, in addition to a control well with no MH1 added. After incubation, the activity was measured in duplicate in 100 μL reaction volumes in a 96-well plate. 50 μM Boc-GRR-AMC substrate was added to a flat bottom black well plate and the enzyme/MH1 mixture was added to initiate the reaction. The activity was read in a SpectraMax M5 spectrophotometer at Ex 355 nm/Em 460 nm. Rates were plotted using Prism (GraphPad Software) and fit to log(inhibitor) vs response, variable slope (four parameters) for IC_{50} determination. Compounds MH2−MH5 and SM1−SM9 were tested in the same manner against ZVP WT, however for these compounds higher concentrations were used to obtain a full IC_{50} curve.

Inhibition Assay. 50 nM ZVP F84A and W61A sample was prepared using activity assay buffer (10 mM Tris, pH 8.5, 20% glycerol, 1 mM CHAPS) and was incubated with increasing concentrations of MH1 (0−4 μM) at room temperature for 1 h. The protease/MH1 mixture was added to 50 μM Boc-GRR-AMC. The fluorescence signal of the substrate was read in a SpectraMax M5 spectrophotometer at Ex 355 nm/Em 460 nm.

Tryptophan FRET Measurements. 0.5 μM protein or no protein as a control, was incubated with 5 μM of the inhibitor (MH or SM compounds) for 1 h at room temperature in 25 mM HEPES, pH 7.5, 75 mM NaCl and 2 mM DTT. Samples were placed in a 96-well black plate and the emission spectrum was recorded using an excitation wavelength of 295 nm. FRET measurements were collected using a SpectraMax M5 spectrophotometer at 25 °C.

Circular Dichroism (CD) Spectroscopy. CD spectra of 5 μM ZVP, ZVP F84A and W61A samples, prepared in 20 mM sodium phosphate buffer, pH 7.4, were measured at 25 °C in 1.0 mm path length quartz cuvette from 180 to 250 nm wavelength using the J-1500 JASCO spectrophotometer. The bandwidth was set at 0.5 mm. Three CD scans were averaged to obtain a single spectrum. Buffer baselines were measured to normalize the CD scans of samples.

Differential Scanning Fluorimetry (DSF). 25 μM protein was incubated with and without 125 μM MH1 (5× excess) for 1 h at room temperature in 25 mM HEPES, pH 7.5, 75 mM NaCl and 2 mM DTT. The reaction was mixed with a final concentration of 5x SYPRO Orange dye before stability was measured in a CFX Connect RT-PCR detection system (BioRad) using a final 50 μL reaction volume in duplicate. Fluorescence was measured at 0.5 °C intervals over the range of 25−95 °C. The thermal melting temperature (Tm) was calculated by fitting the curves to buffer subtracted values using Prism (GraphPad software).

DFT Analysis. All calculations were performed in Gaussian09 with the B3LYP hybrid functional and the split-valence triple-ζ Pople basis set 6-311++G(d,p). Geometry optimization was conducted with an RMS force criterion of 3×10^{-4} a.u. The surrounding solvent was approximated using the polarizable continuum model with H_2O as the implicit solvent. We considered the lowest energy molecular geometries for our analysis, indicated by geometries with strictly positive normal mode vibrational frequencies (Table S1). Mulliken atomic charges were obtained from the geometry optimization output files (Figure S7).

■ ASSOCIATED CONTENT

Supporting Information

The Supporting Information is available free of charge at https://pubs.acs.org/doi/10.1021/acs.biochem.4c00415.

Fluorescence spectra of ZVP and its variants in complex with MH and SM compounds at various concentrations, sequence alignments of flaviviral NS2B-NS3 proteases, models of potential binding sites and orientations for MH1 and details for the for DFT calculations (PDF)

■ AUTHOR INFORMATION

Corresponding Author

Jeanne A. Hardy − *Department of Chemistry, University of Massachusetts Amherst, Amherst, Massachusetts 01002, United States;* orcid.org/0000-0002-3406-7997; Email: jhardy@umass.edu

Authors

Kristalle G. Cruz − *Department of Chemistry, University of Massachusetts Amherst, Amherst, Massachusetts 01002, United States*

Kevin Alexander − *Department of Chemistry, University of Massachusetts Amherst, Amherst, Massachusetts 01002, United States*

Sparsh Makhaik − *Department of Chemistry, University of Massachusetts Amherst, Amherst, Massachusetts 01002, United States*

Complete contact information is available at: https://pubs.acs.org/10.1021/acs.biochem.4c00415

Notes

The authors declare no competing financial interest.

■ REFERENCES

(1) Zimmerman, M.; Ashe, B.; Yurewicz, E. C.; Patel, G. Sensitive assays for trypsin, elastase, and chymotrypsin using new fluorogenic substrates. *Anal. Biochem.* **1977**, *78*, 47−51.

(2) Yusof, R.; Clum, S.; Wetzel, M.; Murthy, H. M. K.; Padmanabhan, R. Purified NS2B/NS3 serine protease of dengue virus type 2 exhibits cofactor NS2B dependence for cleavage of substrates with dibasic amino acids in vitro. *J. Biol. Chem.* **2000**, *275*, 9963−9969.

(3) Blum, G.; Mullins, S. R.; Keren, K.; Fonovič, M.; Jedeszko, C.; Rice, M. J.; Sloane, B. F.; Bogyo, M. Dynamic Imaging of Protease

Activity With Fluorescently Quenched Activity-Based Probes. *Nat. Chem. Biol.* **2005**, *1*, 203−209.
(4) Bogyo, M.; McMaster, J. S.; Gaczynska, M.; Tortorella, D.; Goldberg, A. L.; Ploegh, H. Covalent modification of the active site threonine of proteasomal β subunits and the Escherichia coli homolog HslV by a new class of inhibitors. *Proc. Natl. Acad. Sci. U. S. A.* **1997**, *94*, 6629−6634.
(5) Luo, S. Y.; Araya, L. E.; Julien, O. Protease Substrate Identification Using N-terminomics. *ACS Chem. Biol.* **2019**, *14*, 2361−2371.
(6) Elliott, P. R.; Lomas, D. A.; Carrell, R. W.; Abrahams, J. P. Inhibitory conformation of the reactive loop of α1-antitrypsin. *Nat. Struct. Biol.* **1996**, *3*, 676−681.
(7) Dahlen, J. R.; Jean, F.; Thomas, G.; Foster, D. C.; Kisiel, W. Inhibition of soluble recombinant furin by human proteinase inhibitor 8. *J. Biol. Chem.* **1998**, *273*, 1851−1854.
(8) Riedl, S. J.; Renatus, M.; Schwarzenbacher, R.; Zhou, Q.; Sun, C.; Fesik, S. W.; Liddington, R. C.; Salvesen, G. S. Structural basis for the inhibition of caspase-3 by XIAP. *Cell* **2001**, *104*, 791−800.
(9) Chai, J.; Shiozaki, E.; Srinivasula, S. M.; Wu, Q.; Dataa, P.; Alnemri, E. S.; Shi, Y. Structural basis of caspase-7 inhibition by XIAP. *Cell* **2001**, *104*, 769−780.
(10) Shiozaki, E. N.; Chai, J.; Rigotti, D. J.; Riedl, S. J.; Li, P.; Srinivasula, S. M.; Alnemri, E. S.; Fairman, R.; Shi, Y. Mechanism of XIAP-mediated inhibition of caspase-9. *Mol. Cell* **2003**, *11*, 519−527.
(11) Sun, C.; Cai, M.; Meadows, R. P.; Xu, N.; Gunasekera, A. H.; Herrmann, J.; Wu, J. C.; Fesik, S. W. NMR structure and mutagenesis of the third Bir domain of the inhibitor of apoptosis protein XIAP. *J. Biol. Chem.* **2000**, *275*, 33777−33781.
(12) Lakowicz, J. R. Principles of fluorescence spectroscopy, In *Principles of Fluorescence Spectroscopy*, Lakowicz, J., Ed.; Springer: New York, NY, 2006.
(13) Piston, D. W.; Kremers, G. J. Fluorescent protein FRET: The good, the bad and the ugly. *Trends Biochem. Sci.* **2007**, *32*, 407−414.
(14) Stryer, L. Fluorescence energy transfer as a spectroscopic ruler. *Annu. Rev. Biochem.* **1978**, *47*, 819−846.
(15) Kozachkov, L.; Padan, E. Site-directed tryptophan fluorescence reveals two essential conformational changes in the Na + /H + antiporter NhaA. *Proc. Natl. Acad. Sci. U. S. A.* **2011**, *108*, 15769−15774.
(16) Li, H. H.; Lyles, D. S.; Thomas, M. J.; Pan, W.; Sorci-Thomas, M. G. Structural determination of lipid-bound apoA-I using fluorescence resonance energy transfer. *J. Biol. Chem.* **2000**, *275*, 37048−37054.
(17) Lakowicz, J. R.; Gryczynski, I.; Wiczk, W.; Laczko, G.; Prendergast, F. C.; Johnson, M. L. Conformational distributions of melittin in water/methanol mixtures from frequency-domain measurements of nonradiative energy transfer. *Biophys. Chem.* **1990**, *36*, 99−115.
(18) Zadran, S.; Standley, S.; Wong, K.; Otiniano, E.; Amighi, A.; Baudry, M. Fluorescence resonance energy transfer (FRET)-based biosensors: Visualizing cellular dynamics and bioenergetics. *Appl. Microbiol. Biotechnol.* **2012**, *96*, 895−902.
(19) Sapsford, K. E.; Berti, L.; Medintz, I. L. Materials for Fluorescence Resonance Energy Transfer Analysis: Beyond Traditional Donor−Acceptor Combinations. *Angew. Chem., Int. Ed.* **2006**, *45*, 4562−4589.
(20) Ghisaidoobe, A. B. T.; Chung, S. J. Intrinsic tryptophan fluorescence in the detection and analysis of proteins: A focus on förster resonance energy transfer techniques. *Int. J. Mol. Sci.* **2014**, *15*, 22518−22538.
(21) Vivian, J. T.; Callis, P. R. Mechanisms of tryptophan fluorescence shifts in proteins. *Biophys. J.* **2001**, *80*, 2093−2109.
(22) Cahour, A.; Falgout, B.; Lai, C. J. Cleavage of the dengue virus polyprotein at the NS3/NS4A and NS4B/NS5 junctions is mediated by viral protease NS2B-NS3, whereas NS4A/NS4B may be processed by a cellular protease. *J. Virol.* **1992**, *66*, 1535−1542.
(23) Ruiz-Linares, A.; Cahour, A.; Després, P.; Girard, M.; Bouloy, M. Processing of yellow fever virus polyprotein: Role of cellular proteases in maturation of the structural proteins. *J. Virol.* **1989**, *63*, 4199−4209.
(24) Markoff, L. In vitro processing of dengue virus structural proteins: Cleavage of the pre-membrane protein. *J. Virol.* **1989**, *63*, 3345−3352.
(25) Zhang, L.; Mohan, P. M.; Padmanabhan, R. Processing and localization of Dengue virus type 2 polyprotein precursor NS3-NS4A-NS4B-NS5. *J. Virol.* **1992**, *66*, 7549−7554.
(26) Chambers, T. J.; Grakoui, A.; Rice, C. M. Processing of the yellow fever virus nonstructural polyprotein: A catalytically active NS3 proteinase domain and NS2B are required for cleavages at dibasic sites. *J. Virol.* **1991**, *65*, 6042−6050.
(27) Preugschat, F.; Yao, C. W.; Strauss, J. H. In vitro processing of dengue virus type 2 nonstructural proteins NS2A, NS2B, and NS3. *J. Virol.* **1990**, *64*, 4364−4374.
(28) Lobigs, M. Flavivirus premembrane protein cleavage and spike heterodimer secretion require the function of the viral proteinase NS3. *Proc. Natl. Acad. Sci. U. S. A.* **1993**, *90*, 6218−6222.
(29) Amberg, S. M.; Rice, C. M. Mutagenesis of the NS2B-NS3-Mediated Cleavage Site in the Flavivirus Capsid Protein Demonstrates a Requirement for Coordinated Processing. *J. Virol.* **1999**, *73*, 8083−8094.
(30) Leung, D.; Schroder, K.; White, H.; Fang, N. X.; Stoermer, M. J.; Abbenante, G.; Martin, J. L.; Young, P. R.; Fairlie, D. P. Activity of Recombinant Dengue 2 Virus NS3 Protease in the Presence of a Truncated NS2B Co-factor, Small Peptide Substrates, and Inhibitors. *J. Biol. Chem.* **2001**, *276*, 45762−45771.
(31) Xing, H.; Xu, S.; Jia, F.; Yang, Y.; Xu, C.; Qin, C.; Shi, L. Zika NS2B is a crucial factor recruiting NS3 to the ER and activating its protease activity. *Virus Res.* **2020**, *275*, 197793.
(32) Cruz, K. G.; Hill Eron, M.; Makhaik, S.; Savinov, S.; Hardy, J. A. A Non-Active-Site Inhibitor with Selectivity for Zika Virus NS2B-NS3 Protease. *ACS Infect. Dis.* **2024**, *10*, 412−425.
(33) Zhuang, Y. D.; Chiang, P. Y.; Wang, C. W.; Tan, K. T. Environment-sensitive fluorescent turn-on probes targeting hydrophobic ligand-binding domains for selective protein detection. *Angew. Chem., Int. Ed.* **2013**, *52*, 8124−8128.
(34) Pal, U.; Pramanik, S. K.; Bhattacharya, B.; Banerji, B.; Maiti, N. C. Binding interaction of a novel fluorophore with serum albumins: Steady state fluorescence perturbation and molecular modeling analysis. *SpringerPlus* **2015**, *4*, 548.
(35) Gonzalez, W. G.; Miksovska, J. Application of ANS fluorescent probes to identify hydrophobic sites on the surface of DREAM. *Biochim. Biophys. Acta, Proteins Proteomics* **2014**, *1844*, 1472−1480.
(36) Schönbrunn, E.; Eschenburg, S.; Luger, K.; Kabsch, W.; Amrhein, N. Structural basis for the interaction of the fluorescence probe 8-anilino-1-naphthalene sulfonate (ANS) with the antibiotic target MurA. *Proc. Natl. Acad. Sci. U. S. A.* **2000**, *97*, 6345−6349.
(37) Hilgenfeld, R.; Lei, J.; Zhang, L. The Structure of the Zika Virus Protease, NS2B/NS3pro. *Adv. Exp. Med. Biol.* **2018**, *1062*, 131−145.
(38) Zhang, Z.; Li, Y.; Loh, Y. R.; Phoo, W. W.; Hung, A. W.; Kang, C. B.; Luo, D. Crystal structure of unlinked NS2B-NS3 protease from Zika virus. *Science* **2016**, *354*, 1597−1600.
(39) Lee, H.; Ren, J.; Nocadello, S.; Rice, A. J.; Ojeda, I.; Light, S.; Minasov, G.; Vargas, J.; Nagarathnam, D.; Anderson, W. F.; Johnson, M. E. Identification of novel small molecule inhibitors against NS2B/NS3 serine protease from Zika virus. *Antiviral Res.* **2017**, *139*, 49−58.
(40) Li, Y.; Zhang, Z.; Phoo, W. W.; Loh, Y. R.; Wang, W.; Liu, S.; Chen, M. W.; Hung, A. W.; Keller, T. H.; Luo, D.; et al. Structural Dynamics of Zika Virus NS2B-NS3 Protease Binding to Dipeptide Inhibitors. *Structure* **2017**, *25*, 1242−1250.E3.
(41) Phoo, W. W.; Li, Y.; Zhang, Z.; Lee, M. Y.; Loh, Y. R.; Tan, Y. B.; Ng, E. Y.; Lescar, J.; Kang, C.; Luo, D. Structure of NS2B-NS3 protease from Zika virus after self-cleavage. *Nat. Commun.* **2016**, *7*, 13410.
(42) Lei, J.; Hansen, G.; Nitsche, C.; Klein, C. D.; Zhang, L.; Hilgenfeld, R. Crystal structure of Zika virus NS2B-NS3 protease in complex with a boronate inhibitor. *Science* **2016**, *353*, 503−506.
(43) Li, Y.; Zhang, Z.; Phoo, W. W.; Loh, Y. R.; Li, R.; Yang, H. Y.; Jansson, A. E.; Hill, J.; Keller, T.H.; Nacro, K.; et al. Structural Insights into the Inhibition of Zika Virus NS2B-NS3 Protease by a Small-Molecule Inhibitor. *Structure* **2018**, *26*, 555−564.e3.

https://doi.org/10.1021/acs.biochem.4c00415
Biochemistry 2024, 63, 3300−3309

(44) Liao, F.; Xie, Y.; Yang, X.; Deng, P.; Chen, Y.; Xie, G.; Zhu, S.; Liu, B.; Yuan, H.; Liao, J.; Zhao, Y.; Yu, M. Homogeneous noncompetitive assay of protein via Förster-resonance-energy-transfer with tryptophan residue(s) as intrinsic donor(s) and fluorescent ligand as acceptor. *Biosens. Bioelectron.* **2009**, *25*, 112−117.
(45) Chappell, K. J.; Stoermer, M. J.; Fairlie, D. P.; Young, P. R. Mutagenesis of the West Nile virus NS2B cofactor domain reveals two regions essential for protease activity. *J. Gen. Virol.* **2008**, *89*, 1010−1014.
(46) Lee, W. H. K.; Liu, W.; Fan, J. S.; Yang, D. Dengue virus protease activity modulated by dynamics of protease cofactor. *Biophys. J.* **2021**, *120*, 2444−2453.
(47) Rut, W.; Groborz, K.; Zhang, L.; Modrzycka, S.; Poreba, M.; Hilgenfeld, R.; Drag, M. Profiling of flaviviral NS2B-NS3 protease specificity provides a structural basis for the development of selective chemical tools that differentiate Dengue from Zika and West Nile viruses. *Antiviral Res.* **2020**, *175*, 104731.
(48) Niyomrattanakit, P.; Winoyanuwattikun, P.; Chanprapaph, S.; Angsuthanasombat, C.; Panyim, S.; Katzenmeier, G. Identification of Residues in the Dengue Virus Type 2 NS2B Cofactor That Are Critical for NS3 Protease Activation. *J. Virol.* **2004**, *78*, 13708−13716.
(49) Matusan, A. E.; Kelley, P. G.; Pryor, M. J.; Whisstock, J. C.; Davidson, A. D.; Wright, P. J. Mutagenesis of the dengue virus type 2 NS3 proteinase and the production of growth-restricted virus. *J. Gen. Virol.* **2001**, *82*, 1647−1656.
(50) Matusan, A. E.; Pryor, M. J.; Davidson, A. D.; Wright, P. J. Mutagenesis of the Dengue Virus Type 2 NS3 Protein within and outside Helicase Motifs: Effects on Enzyme Activity and Virus Replication. *J. Virol.* **2001**, *75*, 9633−9643.
(51) Gleason, P. R.; Kelly, P. I.; Grisingher, D. W.; Mills, J. H. An intrinsic FRET sensor of protein-ligand interactions. *Org. Biomol. Chem.* **2020**, *18*, 4079−4084.
(52) Kim, J. H.; Sumranjit, J.; Kang, H. J.; Chung, S. J. Discovery of coumarin derivatives as fluorescence acceptors for intrinsic fluorescence resonance energy transfer of proteins. *Mol. BioSyst.* **2014**, *10*, 30−33.
(53) Talukder, P.; Chen, S.; Roy, B.; Yakovchuk, P.; Spiering, M. M.; Alam, M. P.; Madathil, M. M.; Bhattacharya, C.; Benkovic, S. J.; Hecht, S. M. Cyanotryptophans as Novel Fluorescent Probes for Studying Protein Conformational Changes and DNA-Protein Interaction. *Biochemistry* **2015**, *54*, 7457−7469.
(54) Chen, S.; Fahmi, N. E.; Wang, L.; Bhattacharya, C.; Benkovic, S. J.; Hecht, S. M. Detection of dihydrofolate reductase conformational change by fret using two fluorescent amino acids. *J. Am. Chem. Soc.* **2013**, *135*, 12924−12927.
(55) Lee, M. M.; Peterson, B. R. Quantification of Small Molecule−Protein Interactions using FRET between Tryptophan and the Pacific Blue Fluorophore. *ACS Omega* **2016**, *1*, 1266−1276.
(56) Huang, S. M.; Yang, F.; Cai, B. Y.; He, Q. T.; Liu, Q.; Qu, C. X.; Han, M. J.; Kong, W.; Jia, Y. L.; Li, F.; Yu, X.; Sun, J. P.; Wang, J. Genetically Encoded Fluorescent Amino Acid for Monitoring Protein Interactions through FRET. *Anal. Chem.* **2019**, *91*, 14936−14942.
(57) Kim, Y. M.; Gayen, S.; Kang, C. B.; Joy, J.; Huang, Q.; Chen, A. S.; Wee, J. L. K.; Ang, M. J. Y.; Lim, H. A.; Hung, A. W.; Li, R.; Noble, C. G.; Lee, L. T.; Yip, A.; Wang, Q. Y.; Chia, C. S. B.; Hill, J.; Shi, P. Y.; Keller, T. H. NMR analysis of a novel enzymatically active unlinked dengue NS2B-NS3 protease complex. *J. Biol. Chem.* **2013**, *288*, 12891−12900.

https://doi.org/10.1021/acs.biochem.4c00415
Biochemistry 2024, 63, 3300−3309